Chemical Papers (2020) 74:3169–3182
https://doi.org/10.1007/s11696-020-01149-7

ORIGINAL PAPER

Response surface methodology for heavy metals removal by tioglycolic-modified Zn–Fe layer double hydroxide as a magnetic recyclable adsorbent

Farnaz Movahhedi[1] · Akram Maghsodi[2] · Laleh Adlnasab[2]

Received: 26 December 2019 / Accepted: 30 March 2020 / Published online: 10 April 2020

Abstract
A new nanoadsorbent was synthesized through intercalation of thioglycolic acid (TGA) in the magnetic layered double hydroxide nanocomposite (Fe_3O_4/Zn–Fe LDH/TGA) and used for the removal of heavy metal ions such as Hg^{2+} and Pb^{2+} from aqueous solutions. The morphology and structure of the synthesized nanoadsorbent were investigated by Fourier transform infrared spectroscopy, X-ray diffraction, field-emission scanning electron microscopy and transmission electron microscopy. Also, the quantitative measurements of metal ions were determined using atomic fluorescence spectroscopy. The simultaneous impact of important parameters on the Hg^{2+} removal including pH, adsorbent dosage and removal time were investigated using response surface methodology. Based on the obtained results, pH 5.5 was achieved, and also 9 mg as adsorbent dosage and 30 min for removal time were selected as optimum conditions in Hg^{2+} removal experiments. The adsorption kinetic results fitted well with the pseudo-second-order model, and the R^2 value = 0.991 while the estimated q_e was matched well with the experimental data. Thermodynamic results showed that the adsorption process of Hg^{2+} was endothermic, feasible and spontaneous. Also, the efficiency of the magnetic nanocomposite was investigated for adsorption of the metal ions. The selectivity experiments showed the following order: $Hg^{2+} \ggg Pb^{2+} > Fe^{2+} > Cu^{2+} > Zn^{2+} > Cd^{2+}$. Finally, the obtained results verified the excellent ability of the magnetic nanoadsorbent for Hg^{2+} removal from the aqueous media for at least three times recycle with 90% recovery.

Keywords Heavy metals · Magnetic layered double hydroxide · Central composite design (CCD) · Thioglicolic acid (TGA)

Introduction

Water pollution with heavy metals such as mercury, lead, nickel and cadmium is one of the main environmental problems which can be created by natural processes and a wide range of anthropogenic threats. These heavy metals have been focused because of their hazardous effects for the ecosystem and living organisms. For examples, Hg^{2+}, the common inorganic type of mercury, with properties such as low volatility, easy mobility and high toxicity can be caused various problems, including neurological hurts, blindness, genetic diseases and different disablements (Esfandiyari et al. 2017). The Word Health Organization (WHO) has expressed 1 µg/L as the maximum allowed concentration for Hg^{2+} in drinking water (Asiabi et al. 2018).

One of the best technique for determination of heavy metals such as cadmium, lead, nickel, mercury and chromium is atomic adsorption spectroscopy specially flame, hydride generation and fluorescence methods (Soylak et al. 1997, 1999; Narin et al. 2001).

Up to now, different techniques have been studied for Hg^{2+} removal such as chemical precipitation, ion exchange, membrane separation, coagulation, photocatalysis, ultrafiltration, adsorption and bioadsorption (Sun et al. 2018; Chen et al. 2019; Maia et al. 2019). Among these techniques, adsorption has been studied by many researchers because of high economic advantages, high removal percentage and easy operations.

✉ Laleh Adlnasab
laleh_adlnasab@yahoo.com

[1] Department of Cellulosic Materials and Packaging, Chemistry and Petrochemistry Research Center, Standard Research Institute (SRI), P.O. Box: 31745-139, Karaj, Iran

[2] Department of Chemistry, Chemistry and Petrochemistry Research Center, Standard Research Institute, P.O. Box: 31745-139, Karaj, Iran

Thus, various kinds of adsorbents including clays, carbon nanotubes, activated carbon, polymers, metal oxides, graphene oxide, metal–organic frameworks, aluminum oxide hydroxide, chitosan and biomaterials have been studied for the removal of heavy metals (Li et al. 2019). Among these adsorbents, clay minerals count as good groups of adsorbents due to their high surface area, low cost and active adsorption sites. Nowadays, layered double hydroxides (LDH_s) as mineral clays have been noticed for heavy metals removal (Peligro et al. 2016; Ali et al. 2018; Asiabi et al. 2018).

These materials with porous and layered structure have large surface area which consist positive charge in the layers (such as Zn^{2+}, Mg^{2+}, Ca^{2+}, Ni^{2+}, Fe^{3+}, Al^{3+}) and negative charge (such as Cl^{-1}, NO_3^{-1}, CO_3^{2-}) in the hydrated interlayer spaces. Interlayer anions can be exchanged with various types of organic or inorganic anions through an ion exchange method or surface adsorption. The perfect anion exchange and intercalation properties of LDH_s cause to use them for various applications such as catalyst, sorbents, ion exchange and energy storage (Daud et al. 2016; Wang et al. 2017). The Hg^{2+} removal using LDHs has been well studied in the literatures (Ghasemi et al. 2017; Asiabi et al. 2018; Chen et al. 2019). The adsorption process is reported via two mechanisms: chelation and chemical precipitation. Ricardo Rojas used Ca–Al LDH for the removal of copper, lead and cadmium (González et al. 2014). Also, Zhang et al. (2015) reported synthesis of the magnetite graphene oxide layered double hydroxide composite for the removal of Pb(II) from aqueous solutions. Asiabiei et al. (2017) investigated the selective removal of heavy metal ions by Ni–Cr LDH_s intercalated with the diphenylamine-4-sulfonate, in which showed a selectivity order of $Zn^{2+} < Cu^{2+} \lll Cd^{2+} < Pb^{2+}$ for the adsorption.

However, LDH_s have low selectivity and weak tendency toward heavy metal ions which it is proposed tobe solved by the intercalation of appropriate interlayer anions in the LDH structure (Asiabi et al. 2018). Since, Hg^{2+} is as a Lewis acid; it has a strong binding affinity toward the soft Lewis bases such as thiol functional groups. Thus, thiol-functionalized adsorbents can be used as a promise material for the selective removal of Hg^{2+}. Different thiol functional groups, such as 1-furoyl thiourea urea, dithiocarbamate, benzoyl thiourea, polysulfides and thiol have been studied for the removal of Hg^{2+}, Pb^{2+}, Cd^{2+}, Cu^{2+} from aqueous solutions (Manos and Kanatzidis 2016; Sarma et al. 2016; Sun et al. 2018; Chen et al. 2019; Maia et al. 2019). Actually, LDHs selectivity for Hg^{2+} could be increased by intercalation of the thiol functional groups in the hydrated interlayer spaces, in which has been reported in some of the studies (Ali et al. 2018; Asiabi et al. 2018; Maia et al. 2019). Jawad et al. (2019) studied the selective removal of heavy metals in wastewater using FeMgAl-LDH with different intercalated anions. Also, Asiabi et al. (2018) synthesized the functionalized layered double hydroxide with nitrogen and sulfur co-decorated carbon dots for selective and efficient removal of Hg^{2+} and Ag^{+} ions.

On the other hand, magnetic properties of Fe_3O_4 nanoparticles cause the easy, fast and more accurate separation of nanoadsorbent from the solutions compared to the other methods, only by using a strong magnet (Ghasemi et al. 2017).

Also, experimental design is an efficient method to investigate the effect of all experimental variables, simultaneously. This is carried out by statistical analyzing of the obtained experimental results in which gives some information about the effect of each variable and the interactions among them. Thus, the number of experiments would be reduced and then costs and time would be saved (Rai et al. 2016). Central composite design (CCD) is a cubic, rotatable and independent quadratic design in response surface methodology (RSM) without needing to use a complete three-level factorial experiment (Adlnasab et al. 2017).

In this study, a novel Fe_3O_4/Zn–Fe LDH/TGA nanocomposite was designed in order to combining the magnetic properties of Fe_3O_4 nanoparticles with strong binding affinity of the thiol functional groups toward heavy metal ions for water treatment. The magnetic nanocomposite was characterized by Fourier transform infrared spectroscopy (FTIR), X-ray diffraction (XRD), field-emission scanning electron microscopy (FESEM), energy-dispersive X-ray spectroscopy (EDS) analysis and transmission electron microscopy (TEM). Also, the removal measurements were taken by atomic fluorescence spectroscopy (AFS). Among the different heavy metals, Hg^{2+} was selected as a model. The influence and significance of effective parameters on Hg^{2+} removal were investigated using CCD and RSM, and the optimum value of each parameter was determined. In addition, the efficiency of adsorbent for the removal of the other heavy metal ions (Co^{2+}, Cu^{2+}, Pb^{2+} and Cd^{2+}) was studied. Thermodynamic parameters and adsorption isotherms were investigated in order to track the adsorption process in details.

Results and discussions

Structural and morphological studies

To evaluate the characterization of Fe_3O_4/Zn–Fe LDH/TGA nanocomposite, FT-IR spectroscopy and XRD pattern as well as FESEM, EDS, TEM and VSM were applied. Figure 1a shows the FT-IR spectra of Fe_3O_4/Zn–Fe LDH and Fe_3O_4/Zn–Fe LDH/TGA. The most interesting strong band at 1080 cm^{-1} in Fe_3O_4/Zn–Fe LDH is attributed to the Si–O–Si stretching vibration. The mentioned peak is weaker in Fe_3O_4/Zn–Fe LDH/TGA, probably due to interaction of LDH with TGA. Also, the peak at 574 cm^{-1} is assigned to the vibration of Fe–O bonds in Fe_3O_4 nanoparticles (Thangaraj et al. 2016). The broad peak at 3400 cm^{-1} is assigned to O–H

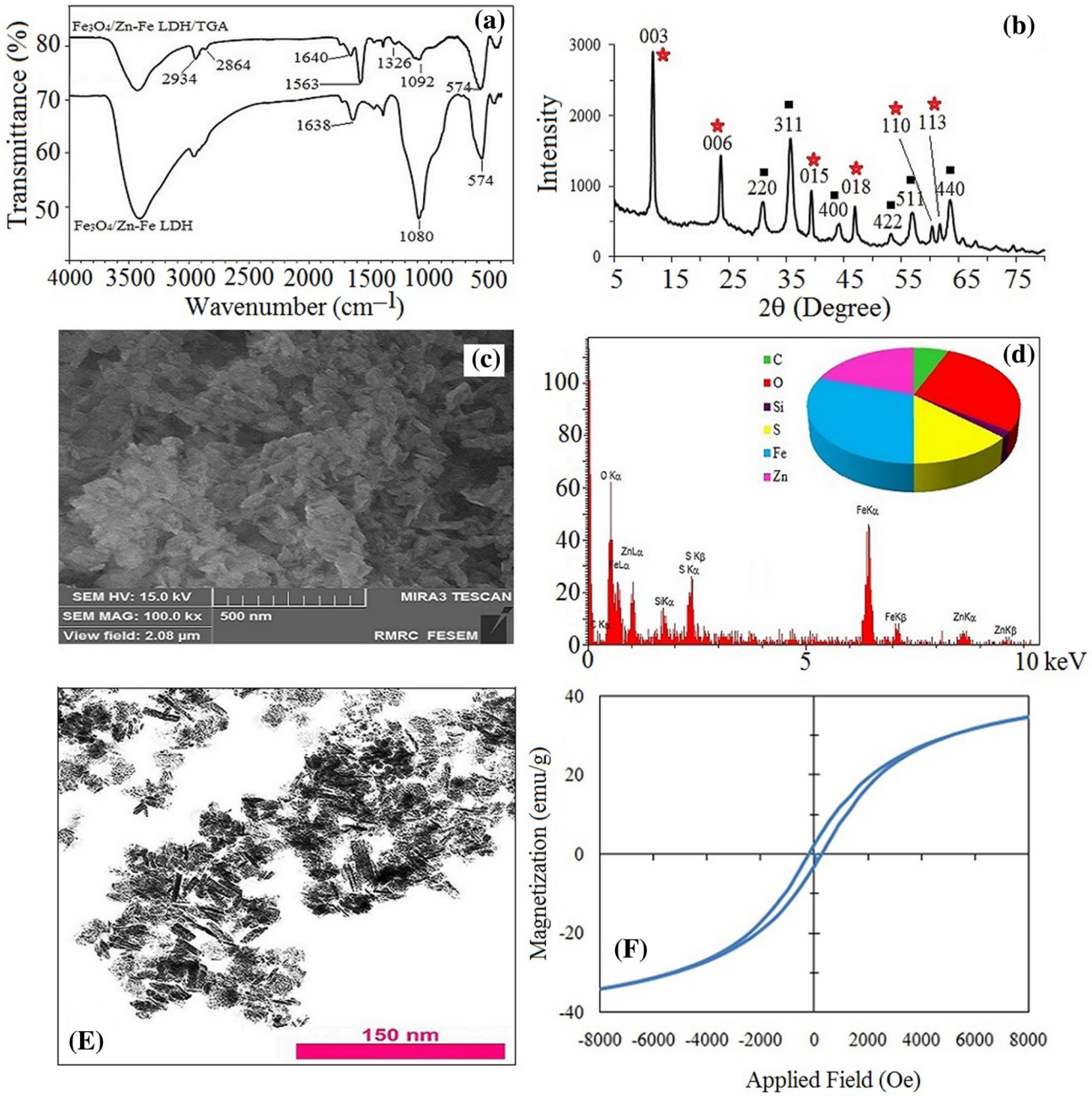

Fig. 1 **a** FTIR spectra of Fe_3O_4/Zn–Fe LDH/TGA and Fe_3O_4/Zn–Fe LDH, **b** XRD patterns of the synthesized adsorbent, **c** FESEM image, **d** point EDS analysis, **e** TEM image and **f** VSM pattern of the Fe_3O_4/Zn–Fe LDH/TGA nanocomposite

stretching vibrations of the LDH surface and would be related to the water molecules trapped in the interlayer spaces (Zhou et al. 2017). The interesting specified peak at 1563 cm^{-1} is related to the asymmetric stretching vibrations of TGA carboxylate groups. Two peaks at 2918.9 cm^{-1} and 2864 cm^{-1} are assigned to asymmetric and symmetric stretching vibrations of the CH_2 groups in Fe_3O_4/Zn–Fe LDH/TGA, respectively (Sumanth Kumar et al. 2016).

The XRD pattern of Fe_3O_4/Zn–Fe LDH/TGA is shown over the diffraction angle of 5°–75° in Fig. 1b. Two specific strong and sharp diffraction peaks at 2θ values 12.0 (003) and 24.0 (006) were assigned to LDH structure. Other diffraction peaks related to LDH are assigned to 37.5 (015), 46.5 (018), 60.5 (110) and 62.0 (113) (Laipan et al. 2017). Also, the specific doublet peaks at 60.5° and 62.0° are observed for LDH structures. In Fig. 1b, the other diffraction peaks such as 2θ values 27.0 (220), 36.0 (311), 44.5 (400),

54.0 (422), 57.0 (511) and 63.5 (440) are confirmed existence of the Fe_3O_4 nanoparticles in the structure of Fe_3O_4/Zn–Fe LDH/TGA (Yan et al. 2015).

The morphology and elemental percent of the Fe_3O_4/Zn–Fe LDH/TGA were investigated by FESEM and the point energy-dispersive X-ray spectroscopy (EDS) (Fig. 1c, d). According to the FESEM result, the layered structure of the LDH was created, while aggregated due to Fe_3O_4 NPs in the structure. The energy-dispersive X-ray spectroscopy (EDX) analyses of the intercalated sample are showed loading of 0.42 mmol/g thioglycolic acid moiety, corresponding to the S content of 1.33%.

TEM micrographs were applied to confirm the morphology and layers thickness of the Fe_3O_4/Zn–Fe LDH/TGA. As shown in Fig. 1e, the synthesized nanocomposite exists in the layered form, in which the thickness of the layers is distributed in the range of 10–15 nm. TEM confirms FESEM images and successful synthesis of Fe_3O_4/Zn–Fe LDH/TGA with exfoliated/intercalated structure.

The magnetization curves of the Fe_3O_4/Zn–Fe LDH/TGA nanocomposite recorded with VSM are illustrated in Fig. 1f. The magnetization of the nanocomposite would approach the saturation value when the applied magnetic field increases to 8000 Oe. The saturation magnetization of the nanocomposite is 36.80 emu/g in which shows suitable efficiency for magnetic separation.

Removal condition optimization and Response surface methodology

In this study, central composite design was applied to design a group of tests for investigation of effective parameters on Hg^{2+} removal and their interactions, in which the optimum values for each parameter was obtained. Also, the interactions between parameters and the correlation between parameters and response could be studied with the least number of experiments by CCD. The parameters including pH (A), adsorbent dosage (B) and removal time (C) were selected as the effective parameters. Based on the CCD, the removal tests (19 runs, Table 1) were carried out using the synthesized adsorbent. The removal percentage ($R\%$) under experimental conditions was as the response in this study. The initial tests showed that the synthesized Fe_3O_4/Zn–Fe LDH/TGA nanocomposite has higher affinity toward the removal of Hg^{2+} compared to the Pb^{2+}. Therefore, the study focused on the optimization of the Hg^{+} removal using the Fe_3O_4/Zn–Fe LDH/TGA nanocomposite as an adsorbent.

The analysis of variance (ANOVA) demonstrates the mathematical relation between effective parameters and response using the quadratic model, P-values and the F-values for Hg^{2+} removal. If P value be less than 0.05 in the ANOVA, and then, the parameter would be a statistical significance at a 95% confidence level. Actually, the statistical significance of each parameter, their interactions and the dependency of responses to parameters are calculated at a 95% confidence level (Roosta et al. 2015; Zare-Dorabei et al. 2016). The experimental relation between Hg^{2+} removal percentage ($R\%$) and independent parameters is shown in Eq. (1):

$$\begin{aligned} R\% = & -260.823 + 65.505 \times (\text{pH}) + 20.868 \times (\text{adsorbent dosage}) + 5.843 \times (\text{Removal time}) \\ & - 6.087 \times (pH)^2 + 0.65 \times \left[(\text{pH solution}) \times (\text{adsorbent dosage})\right] - 0.158 \times \left[(\text{pH}) \times (\text{Removal time})\right] \\ & - 1.410 \times (\text{adsorbent dosage})^2 + 0.033 \times \left[(\text{adsorbent dosage}) \times (\text{Removal time})\right] - 0.088 \times (\text{Removal time})^2 \end{aligned} \quad (1)$$

The obtained significant terms in the model with their P and F-values are listed in ANOVA table (Table 2). According to the results, the P-values corresponding to terms A, B, AA, BB and CC are less than 0.05 (< 0.0001 for B, AA and CC) which ndicate that the suggested model and the terms are statistically significant at the 95.0% confidence level (Ghitescu et al. 2015; Tekin et al. 2015; Maran et al. 2016; Rai et al. 2016) and the terms C, AB, AC and BC are more than 0.05 that they are insignificant terms at the 95.0%

Table 1 Removal conditions for each run for CCD

Run	A: pH	B: adsorbent dosage (mg)	C: removal time (min)
1	7	3	15
2	3	3	15
3	3	3	45
4	5	5.5	30
5	5	9.5	30
6	3	8	45
7	8.5	5.5	30
8	1.5	5.5	30
9	5	5.5	55
10	5	1.5	30
11	5	5.5	30
12	5	5.5	30
13	7	8	45
14	7	8	15
15	5	5.5	5
16	7	3	45
17	5	5.5	30
18	3	8	15
19	5	5.5	30

Table 2 Analysis of variance (ANOVA) for the removal experiments

Source	Sum of squares	D_f	Mean square	F-value	P value	Significance
A: pH	676.465	1	676.465	9.35	0.0136	Significant
B: adsorbent dosage	7572.49	1	7572.49	104.64	< 0.0001	Significant
C: removal time	2.09836	1	2.09836	0.03	0.8686	Not significant
AA	9260.66	1	9260.66	127.97	< 0.0001	Significant
AB	84.5	1	84.5	1.17	0.3080	Not significant
AC	180.5	1	180.5	2.49	0.1487	Not significant
BB	906.277	1	906.277	12.52	0.0063	Significant
BC	12.5	1	12.5	0.17	0.6874	Not significant
CC	5170.01	1	5170.01	71.44	< 0.0001	Significant
Total error	651.292	9	72.3658			
Total (corr.)	21,887.3	18				
R-squared = 97.13%				Standard error of est. = 8.5		
Adjusted R-squared = 94.1%				Mean absolute error = 4.5		

confidence level. Also, the high values of R-square (97.13%) and adjusted R-square (94.1%) indicate the accuracy and excellent fitting of the suggested model with obtained experimental data.

The Pareto chart and the main effects of any parameter are shown in Fig. 2a. The Pareto chart describes that the most significant parameters affecting the response on the synthesized adsorbent are quadratic term of pH (AA) followed by adsorbent dosage (B), quadratic term of removal time (CC), quadratic term of adsorbent dosage (BB) and pH (A) which among them, A and B terms are positive effect on Hg^{2+} removal.

The main effect of any parameters on Hg^{2+} removal is shown separately in Fig. 2b which indicates that the adsorbent dosage has positive effect, i.e., by increasing the adsorbent dosage from 3 to 8 mg, the Hg^{2+} removal percentage

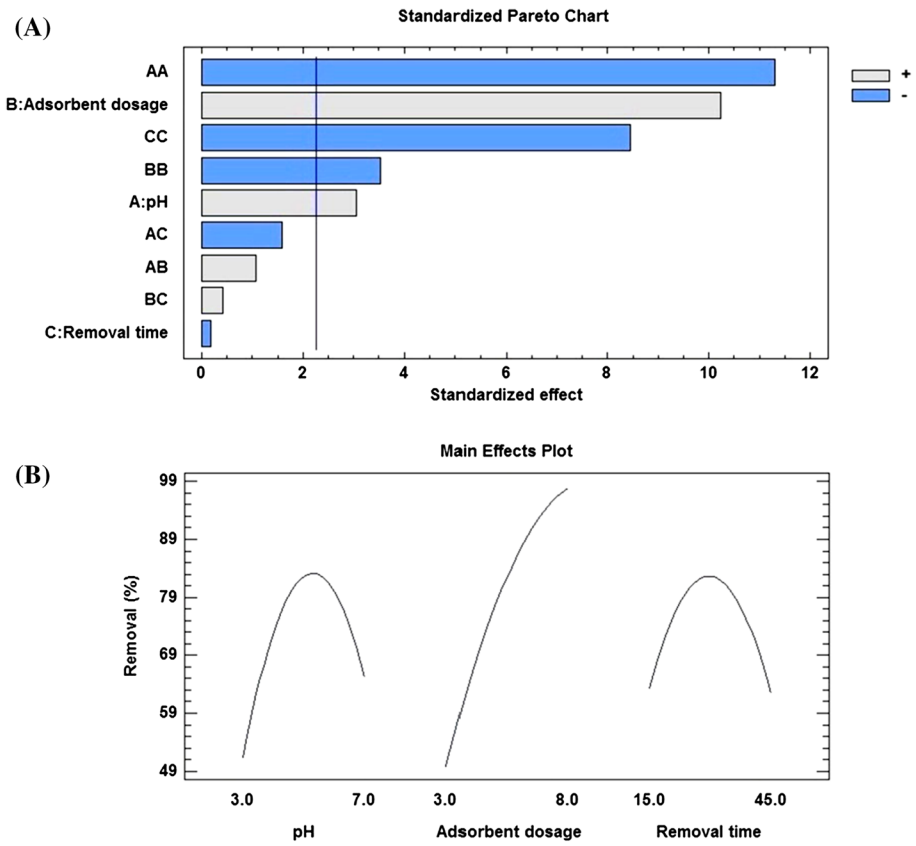

Fig. 2 **a** Standardized Pareto chart and normalization at 95% significance and **b** the main effects of parameters on Hg^{2+} removal

would be increased significantly, while the response would be decreased by increasing the pH and removal time.

Response surface methodology (RSM)

The response surface methodology (RSM) is utilized based on the CCD to obtain the optimum values of each effective parameter. The effects of independent parameters and their interactions on Hg^{2+} removal (*R*%) are demonstrated with 3D response surfaces in Fig. 3a–c. In each plot, the main parameters are varied from their low level to their highest level, while all the other parameters are hold constant at their optimum value.

Effect of pH

The effect of pH (range 3–7), its interaction with adsorbent dosage (range 3–8 mg) and removal time (range 15–45 min) are presented in Fig. 3a, b, respectively. According to the Pareto chart, both interactions could not be significant in Hg^{2+} removal. The adsorption or removal process for heavy metals is controlled strongly by solution pH, especially for As^{3+}, Cd^{2+} and Hg^{2+}, which could be related to the effect of pH on the adsorbent surface charge (different forms) and solution chemistry of heavy metals under various pH values (Zhang et al. 2013).

As it can be seen from Fig. 3a, the response (*R*%) increased gradually with increasing pH from 3 to 5.5 and then decreased. This phenomenon can be related to this fact that at lower pH, because of the high concentrations of H^+ ions in the solution, there would be a competition between H^+ and Hg^{2+} ions toward the adsorbent surface. Actually, the surface of the adsorbent is protonated and covered with H^+ ions at low pH values, in which prevents Hg^{2+} ions to be connected to the active sites of the nanoadsorbent, by the strong repulsive forces between H^+ and Hg^{2+} ions (Moradi 2011). These results are confirmed by the surface complex formation theory, in which the competition between H^+ and Hg^{2+} ions for the adsorption sites decreases by increasing the pH. Also, increasing the pH is concluded in the adsorbent surface negative charge, and thus, electrostatic interactions between the adsorbent (with negative surface charge) and Hg^{2+} ions would be increased and the response would be enhanced (Montgomery 1997; Maghsodi and Adlnasab 2019).

It would be proposed that the adsorption sites of the nanoadsorbent are deprotonated with increasing the pH value and become free for more adsorption of Hg^{2+} ions (Li et al. 2013; Roosta et al. 2014). At pH levels higher than 5.5, the response decreases sharply, in which can be related to the deposition of Hg^{2+} ions in the form of $Hg(OH)_3^-$ and $Hg(OH)_4^-$ complexes. These complexes are soluble in water and could not be maintained on the adsorbent surface (Shadbad et al. 2011; Moustafa et al. 2014; Tahermansouri et al. 2014). As a whole, increasing the pH values in the basic region decreases the Hg^{2+} removal percentage and has negative effect on the removal efficiency (Alimohammady et al. 2017). According to the obtained results, pH 5.5 was chosen as the optimum pH with higher Hg^{2+} removal percentages.

Effect of adsorbent dosage

The effect of adsorbent dosage for Hg^{2+} removal percentage was investigated in the range of 3–8 mg, and the results are demonstrated in Fig. 3a, c. Obviously, with changing the adsorbent dosage from 3 to 9 mg, the response rate increased and achieved to the maximum value in the 9 mg adsorbent dosage. So, 9 mg was selected as optimum value for adsorbent dosage in which it could be due to the presence of the more available active sites for adsorption of Hg^{2+} ions. Also, the maximum response with the highest adsorbent dosage was obtained at pH ~ 5.5, in which probably more deprotonated adsorption sites are achievable.

Effect of removal time

The removal (stirring) time is another important parameter in the removal process, which affects on the interaction between the adsorbent and adsorbate. The 3D interaction plots of removal time (15–45 min)/pH and removal time/adsorbent dosage are shown in Fig. 3b, c, respectively. The response rate increased by increasing the removal time reached the maximum value at 30 min and then reduced. Actually, stirring causes better dispersion of the adsorbent in the solution concluded in increasing the mass transfer and diffusion coefficient. So, more free and active adsorption sites for Hg^{2+} ions will be accessible by decreasing the removal time (Jamshidi et al. 2015; Zare-Dorabei et al. 2016).

Also, the adsorbent active surface sites would be saturated at higher removal times and then decrease the Hg^{2+} desorption values in the removal process (Zare-Dorabei et al. 2016). Hence, 30 min was selected as the optimum removal time giving the maximum response.

Based on the RSM results, pH 5.5, 9 mg as adsorbent dosage and 30 min removal time were selected as the optimum conditions in the Hg^{2+} removal experiments on the synthesized Fe_3O_4/Zn–Fe LDH/TGA adsorbent.

Zeta potential analysis

In order to confirm the adsorption mechanism, the zeta potential on the surface of nanocomposite was determined to obtain the zero point charge (pH_{PZC}). According to the

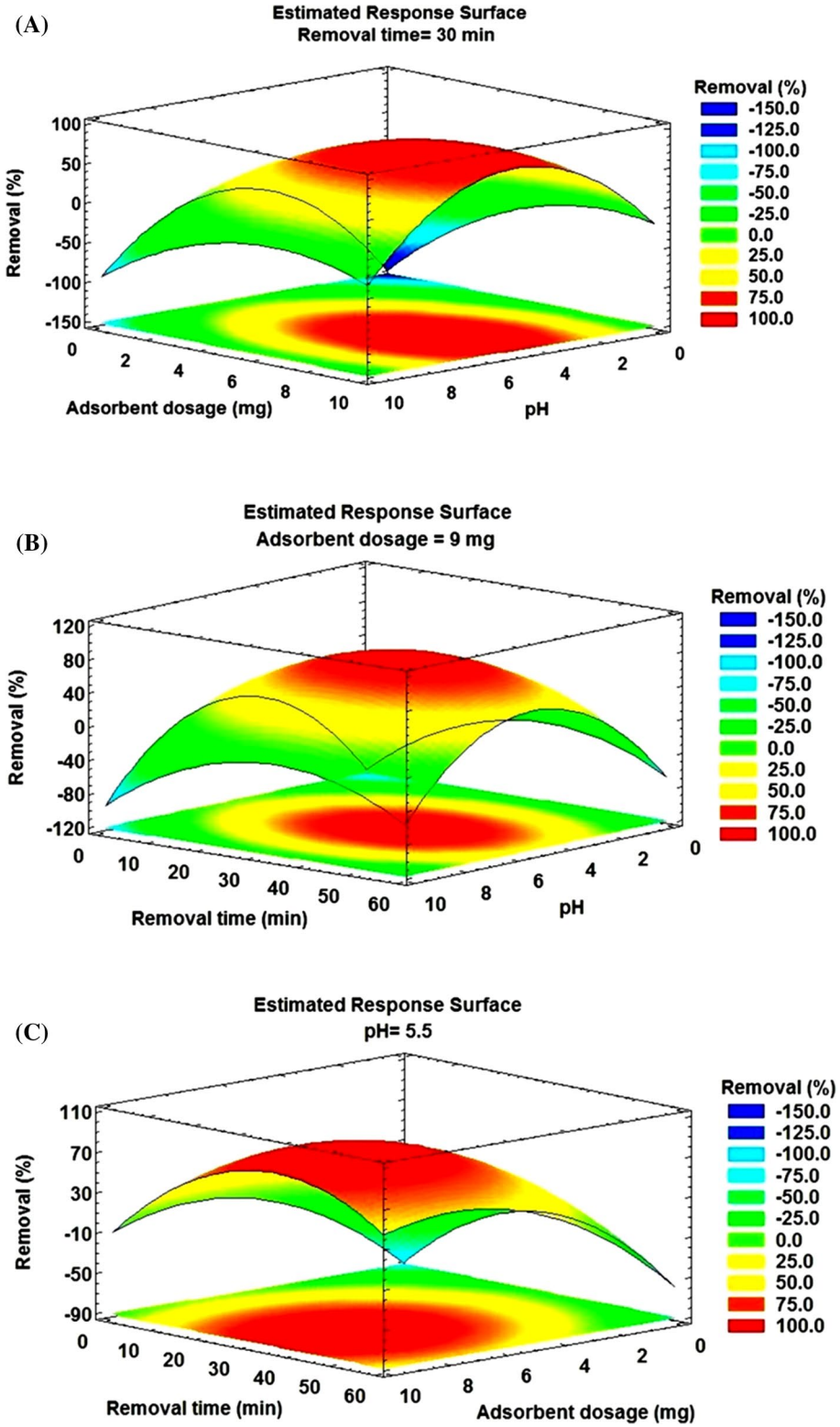

Fig. 3 3D response surfaces plots for parameters of **a** pH solution-adsorbent dosage, **b** pH solution-removal time and **c** adsorbent dosage-removal time

results in Fig. 4, the zeta potential value of nanocomposite decreased with the increase in solution pH, and the pH_{PZC} was about 3.5. The surface of the nanocomposite has the zero electrical charge density in the pH_{PZC}. The surface has positive charge at $pH < pH_{PZC}$, in which it has negative charge at $pH_{PZC} < pH$. So, the results of the zeta potential confirm the negative charge on surface nanocomposite at pH 5.5.

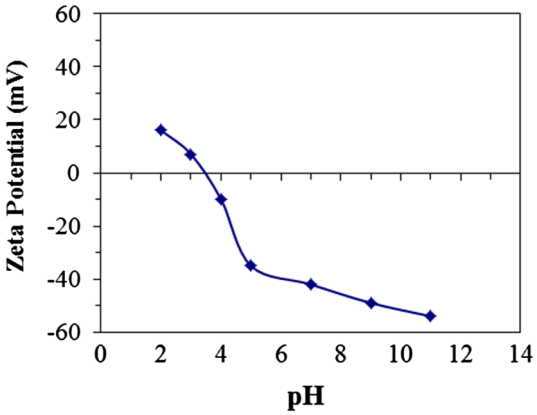

Fig. 4 Zeta potential of Fe_3O_4/Zn–Fe LDH/TGA versus pH

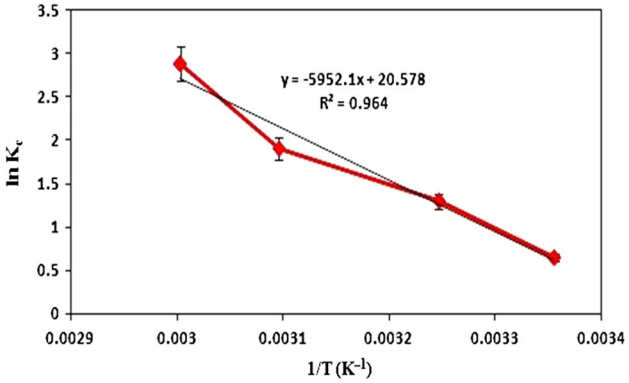

Fig. 5 Effect of temperature on the removal of Hg^{2+} by Fe_3O_4/Zn–Fe LDH/TGA

Thermodynamic studies

The thermodynamic parameters such as Gibbs free energy change (ΔG°), entropy change (ΔS°) and enthalpy change (ΔH°) were applied to describe the possibility and nature of the adsorption process on the Fe_3O_4/Zn–Fe LDH/TGA nanocomposite at different temperatures and are calculated according to Eqs. (2) and (3):

$$\Delta G^{\circ} = -RT \ln K \tag{2}$$

$$\ln K = -\frac{\Delta G^{\circ}}{RT} = -\frac{\Delta H^{\circ}}{RT} + \frac{\Delta S^{\circ}}{R} \tag{3}$$

where K (q_e/C_e), T and R are the equilibrium constant at different temperatures, the absolute temperature (K) and the gas constant (8.3145 J mol^{-1} K^{-1}), respectively (Liu et al. 2013). ΔS° and ΔH° are obtained from the intercept and slope of the plot of lnK versus 1/T, respectively (Fig. 5). The obtained ΔH°, ΔS° and ΔG° at different temperatures are presented in Table 3. The negative value for ΔG° expresses that the adsorption of Hg^{2+} on the nanoadsorbent is a feasible and spontaneous process and it would be even more negative by increasing the temperature implying that the adsorption process increases at higher temperatures.

The negative value for ΔH° confirms the adsorption process to be exothermic. Also, the positive value of ΔS° confirms the high tendency of the Fe_3O_4/Zn–Fe LDH/TGA nanoadsorbent toward Hg^{2+} ions, in which increases during the adsorption process (Liu et al. 2013; Periyasamy et al. 2017).

Kinetic studies

The kinetic isotherms of an adsorption process are important and describe the effect of nanoadsorbent in rate of the adsorption. The kinetic experiments were carried out by adding the Fe_3O_4/Zn–Fe LDH/TGA nanoadsorbent into 10 mL of Hg^{2+} standard solution with concentrations of 10 mg/L at pH 5.5 and contact times ranging from 5 to 60 min at 25 °C.

The pseudo-first-order and pseudo-second-order kinetic models were used to investigate the adsorption kinetic model (Zhang et al. 2016). The linear form of the pseudo-first-order kinetic equation is given as follows (Eq. 4):

$$\log\left(q_e - q_t\right) = \log q_e - \frac{K_1}{2.303}t \tag{4}$$

where q_e and q_t are adsorption capacities (mg g^{-1}) of the adsorbent at the equilibrium time and at t (min) time, respectively, and K_1 is the rate constant of the pseudo-first-order model. By plotting the $\log(q_e - q_t)$ versus time (Fig. 6a) and calculating the intercept and slope, the q_e and K_1 are achieved, respectively.

Also, the linear pseudo-second-order model is used according to Eq. (5) (Zhang et al. 2016):

$$\frac{t}{q_t} = \frac{1}{K_2 q_e^2} + \frac{1}{q_e}t \tag{5}$$

where K_2 (g/(mg min)) is the rate constant of pseudo-second-order adsorption model.

Table 3 Thermodynamic data for the removal of Hg^{2+} by Fe_3O_4/Zn–Fe LDH/TGA adsorbent

Temperature (K)	K_c (L/g)	ΔG° (kJ/mol)	ΔH° (kJ/mol)	ΔS° (J/(mol K))
298	1.90	−50.22		
308	3.64	−50.25	−49.486	2.4751022
323	6.67	−50.29		
333	17.78	−50.31		

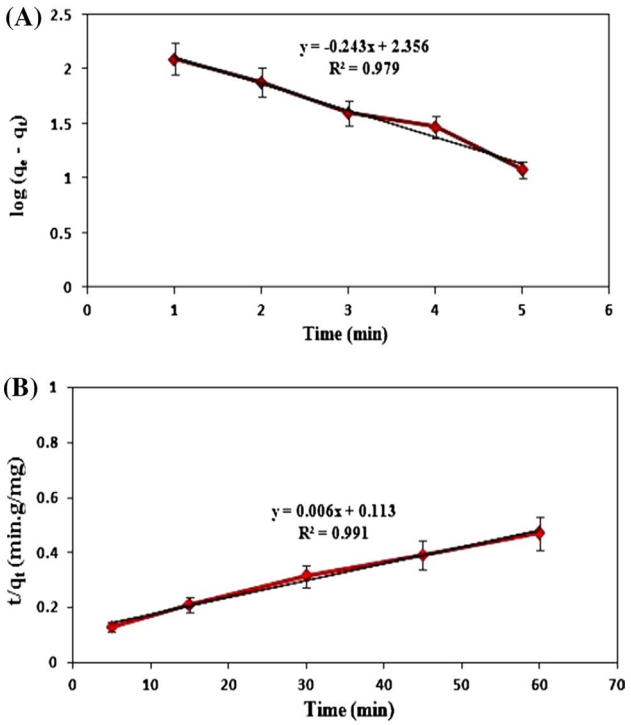

Fig. 6 **a** Linear plots of pseudo-first-order kinetic and **b** pseudo-second-order kinetic models

As it can be seen (Fig. 6a, b), the adsorption process of Hg^{2+} on Fe_3O_4/Zn–Fe LDH/TGA adsorbent has the best fit with pseudo-second-order model data in comparison with linear pseudo-first-order model under the experimental conditions. Also, the pseudo-second-order model presents higher R^2 value (0.991) and the estimated q_e is matched well with the experimental data. The values of kinetics parameters for both models are given in Table 4.

Maximum capacity

For understanding the maximum adsorption capacity (q_m) of the adsorbent, 9 mg Fe_3O_4/Zn–Fe LDH/TGA nanoadsorbent was added to the 20 mg/L Hg^{2+} standard solution (100 ml) under optimum conditions (pH 5.5, time = 30 min) and residual Hg^{2+} value in the solution was measured with AFS. The q_m is calculated according to the following Eq. (6) (Duan et al. 2015):

$$q_m = \frac{(C_0 - C_e)V}{m} \quad (6)$$

where C_0 and C_e (mg/L) are the initial and final concentrations of Hg^{2+} ions in the solution, respectively. Also, V and m are the solution volume (L) and adsorbent dosage (g) values, respectively. The obtained maximum adsorption capacity was achieved 198.5 mg/g for Fe_3O_4/Zn–Fe LDH/TGA nanoadsorbent.

Adsorbent reusability

In the adsorption process, reducing cost of the tests depends to the reusability of the adsorbents. For evaluation of the reusability, the desorption test of Hg^{2+} from adsorbent was rendered with 10 mL HNO_3 (0.5 M) as an eluent. Continuously, this adsorbent was used for at least three times adsorption and desorption with 90% recovery.

Real sample analysis

Three different real water samples (Zarshouran mine) were used to investigate the efficiency of the Fe_3O_4/Zn–Fe LDH/TGA adsorbent for Hg^{2+} removal at optimum conditions (pH 5.5, adsorbent dosage = 9 mg and removal time = 30 min). The samples were spiked with different concentrations of Hg^{2+} standard solutions (100 and 250 µg/L) and the nanoadsorbent was added into these solutions. Removal percentage (%) was calculated by Eq. (7):

$$\text{Removal}\,(\%) = \frac{C_{\text{total}} - C_{\text{residual}}}{C_{\text{total}}} \times 100 \quad (7)$$

where C_{total} is sum of the initial concentration of Hg^{2+} in the real samples with the added (spiked) Hg^{2+} concentration and C_{residual} is the residual concentration of Hg^{2+} after removal. The obtained results showed that the removal percentages for the samples were in the range of 94% and 99% (Table 5). The high removal efficiencies showed that the synthesized Fe_3O_4/Zn–Fe LDH/TGA nanoadsorbent could be presented as a suitable option for Hg^{2+} removal from different aqueous solutions.

Table 4 Parameters of pseudo-first-order and pseudo-second-order kinetic for Hg^{2+} adsorption on the Fe_3O_4@Zn–Fe LDH@TGA adsorbent

Temperature (°C)	Lagergren pseudo-first-order kinetics			Pseudo-second-order kinetics		
	q_e (mg/g)	K_1 (g/(mg min))	R^2	q_e (mg/g)	K_2 (g/(mg min)	R^2
25	145.5	0.04	0.979	166.7	0.0003	0.991

Comparing of Fe_3O_4/Zn–Fe LDH/TGA with other adsorbents

The efficiency of the Fe_3O_4/Zn–Fe LDH/TGA nanoadsorbent in comparison with the other adsorbents for Hg^{2+} adsorption is listed in Table 6. The obtained results show the significant performance of the synthesized nanoadsorbent for Hg^{2+} adsorption in comparison with the other adsorbents. Most of them have q_m lower than this adsorbent. Therefore, Fe_3O_4/Zn–Fe LDH/TGA nanoadsorbent can be proposed as a new and efficient adsorbent for the removal of Hg^{2+} from polluted waters.

In addition, all of the mentioned experimental tests were investigated to know the efficiency of the Fe_3O_4/Zn–Fe LDH/TGA nanoadsorbent for adsorption some of the other metal ions. The results showed that the adsorption order is: $Hg^{2+} \ggg Pb^{2+} > Fe^{2+} > Cu^{2+} > Zn^{2+} > Cd^{2+}$. Thus, the nanoadsorbent can be used for removal of these ions from aqueous solutions and this is one of the adsorbent advantages.

Table 5 Analysis of Hg^{2+} in spiked real samples at different concentrations

Sample	$C_{initial}$ (μg/L)	C_{added} (μg/L)	Removal (%)	RSD (%)
Tap water	–	100	98.5	≤5.0
	–	250	96.0	≤5.0
Well water	–	100	97.5	≤5.0
	–	250	96.9	≤5.0
Waste water	65.0	–	89.2	≤7.5
	–	100	96.5	≤6.5
	–	250	95.4	≤6.5

Conclusion

The magnetic Zn–Fe LDH/TGA nanocomposite was synthesized through the LDH formation in the presence of thioglicolic acid (TGA) and then magnetization of the complex with Fe_3O_4/SiO_2 nanoparticles. Then, the as-synthesized nanocomposite is applied as an adsorbent for heavy metals removal (Hg^{2+}, Pb^{2+}, Cd^{2+}) from aqueous solutions. The optimum conditions for Hg^{2+} removal including pH 5.5, adsorbent dosage = 9 mg and removal time = 30 min were obtained by CCD and RSM. The adsorption kinetic results fitted well with the pseudo-second-order model. Thermodynamic results showed that the adsorption of Hg^{2+} on Fe_3O_4/Zn–Fe LDH/TGA is an endothermic, feasible and spontaneous process. The real samples results showed that the synthesized nanocomposite has excellent ability to remove Hg^{2+} from aqueous media with 90% recovery percentage. The selectivity of adsorbent toward some heavy metal ions shows the following order: $Hg^{2+} \ggg Pb^{2+} > Fe^{2+} > Cu^{2+} > Zn^{2+} > Cd^{2+}$.

Experimental

Materials

Thioglicolic acid (TGA), sodium hydroxide (NaOH), Fe $(NO_3)_3.9H_2O$, Zn $(NO_3)_2.4H_2O$, 2-propanol, ethylene glycol $((CH_2OH)_2)$, $FeCl_3 \cdot 6H_2O$, $FeCl_2 \cdot 4H_2O$, ammonia solution (25 wt%), ethanol (96%), n-propanol, standard solutions of Hg^{2+}, Pb^{2+}, Cd^{2+} and Cu^{2+}(1000 mg/Lin HNO_3 10% v/v) were purchased from Merck (Darmstadt, Germany). Tetraethyl orthosilicate (TEOS) was supplied by Sigma-Aldrich (St. Louis, MO, USA). The standard working solution of

Table 6 Comparison of the Fe_3O_4/Zn–Fe LDH/TGA adsorbent with other adsorbents reported in the literature for Hg^{2+} removal

Adsorbent	q_{max}(mg/g)	References
FeMnOOH	12	Kokkinos et al. (2015)
Graphene oxide/Fe–Mn composite	33	Tang et al. (2016)
δ-FeOOH	35	Maia et al. (2019)
Bamboo	2.71	Tan et al. (2011)
Fe_3O_4-GS	23.1	Maia et al. (2019)
Magnetic mesoporous silica composites	19.8	Song et al. (2011)
Fe_3O_4@SiO_2-SH nanoparticles	90.0	Wang et al. (2016)
Titanium dioxide nanoparticles	90.9	Afshar et al. (2017)
SH-Fe_3O_4-NMP	256.4	Pan et al. (2012)
EDTA-magnetic graphene oxide	268.4	Cui et al. (2015)
Polystyrene coated $CoFe_2O_4$ particles	86.9	Jainae et al. (2015)
Curcumin-based magnetic nanocomposite (CMNC)	144.9	Naushad et al. (2019)
Fe_3O_4/Zn–Fe LDH/TGA	198.5	This study

Hg^{2+} (10 mg/L) was prepared from dilution of stock solution with deionized water.

Instruments

Hg^{2+} removal measurements were taken using atomic fluorescence spectroscopy (AFS, XGY-1011A, China) which equipped with high-intensity Hg hollow-cathode lamp (current intensity: 50–60 mA) and a quartz tube as atomizer where argon (Ar) flow is carried out in the volatile species. A digital pH meter (Mettler Toledo, model M225, Swiss, https://www.mt.com) was used for the pH measurements. A 50/60-Hz, 350-W ultrasonic bath with temperature control (Euronda, Eurosonic 4D, 320 V, Italy, http://www.prosystem.euronda.com) was applied for dispersing the materials in solutions. The Fourier-transform infrared (FTIR) spectra of the adsorbent were recorded by the Bruker Vertex 70 (http://www.bruker.com) in the frequency range of 400–4000 cm^{-1}. The magnetic nanocomposite was characterized by the X-ray diffraction measurements on a X-ray diffractometer (X'Pert PRO MPD, PANalytical Company, Netherlands, https://www.malvernpanalytical.com) over the 2θ range from 10° to 80° using Cu K_α radiation ($\lambda = 1.54060$ Å). The morphology of the nanocomposite was studied by field-emission scanning electron microscopy (FESEM, MIRA3, TESCAN-XMU, https://www.tescan.com). The chemical composition of the nanocomposite was determined by an energy-dispersive X-ray system (SIRIUS SD, scientific instrument, the UK, https://www.rayspec.co.uk). VSM analysis was performed to confirm magnetic properties of nanocomposite by a vibrating sample magnetometer (VSM) (AGFM/VSM 3886 Kashan, Iran) with an applied field between − 8000 and 8000 Oe at room temperature. Zeta potentials measurements were taken by SZ-100 Horiba scientific (Kyoto, Japan, https://www.horiba.com).

Synthesis of Fe_3O_4/Zn–Fe LDH/TGA

Synthesis of Zn–Fe LDH/TGA

At the present work, Zn–Fe LDH was synthesized in the presence of TGA as a source of sulfur. Firstly, 0.24 g of TGA was added into 30 ml pre-boiled deionized water (as water without CO_2) at a three-necked flask in an oil bath at 65 °C and the solution pH was adjusted at 10 with addition of 1 mol/L NaOH solution. On the other hand, 0.925 g (0.0023 mol) Fe $(NO_3)_3.9H_2O$ and 0.898 g (0.0034 mol) Zn $(NO_3)_2.4H_2O$ (molar ratio = 1:1.5) were dissolved in 15 mL deionized water, 15 mL 2-propanol and 6 mL ethylene glycol. The prepared solution was added dropwise into the TGA solution, while the pH was maintained constant at 10 with addition of 1 mol/L NaOH solution. The resulting slurry was stirred vigorously at 70 °C for 24 h and followed by aging at the same temperature for 12 h. Finally, the synthesized Zn–Fe LDH/TGA was centrifuged and washed with pre-boiled deionized water several times and dried in a vacuum oven at 70 °C overnight.

Synthesis of Fe_3O_4@SiO_2

The synthesis of Fe_3O_4 nanoparticles was performed by the in situ chemical co-precipitation method (Maghsodi et al. 2018). Briefly, $FeCl_2.4H_2O$ and $FeCl_3.6H_2O$ were dissolved in the pre-boiled deionized water at 50 °C under argon atmosphere. The ammonia solution was added to this solution and heated at 80 °C for desired time. The magnetic nanoparticles were obtained that washed with ethanol/water. These nanoparticles were coated with a thin layer of silica microspheres by addition of 17 mL of TEOS to the mixed solution of pre-boiled deionized water, n-propanol and prepared Fe_3O_4 nanoparticles under argon atmosphere and vigorous stirring for 17 h at 38 °C. Finally, the obtained Fe_3O_4@SiO_2 nanoparticles were washed and dried at 75 °C overnight.

Magnetization of Zn–Fe LDH/TGA

For magnetizing of the Zn–Fe LDH/TGA, 0.36 g the as-synthesized Zn–Fe LDH@TGA and 45 mg Fe_3O_4@SiO_2 were dispersed in the pre-boiled deionized water and ultrasound for 6 h. Then, the suspension was separated with an external magnet and washed with the pre-boiled deionized water three times and dried in a vacuum oven at 70 °C overnight. The final nanocomposite was named as Fe_3O_4/Zn–Fe LDH/TGA.

Synthesis of Fe_3O_4/Zn–Fe LDH

For investigation of TGA effect on Hg^{2+} removal, the Fe_3O_4/Zn–Fe LDH nanocomposite was synthesized without intercalated TGA according to the method described for the synthesis of Fe_3O_4/Zn–Fe LDH/TGA.

Removal experiments

The simultaneous effects of important parameters and their interactions on the Hg^{2+} removal such as pH, adsorbent dosage and removal time were investigated with CCD and RSM. The CCD and RSM were applied by using the STATGRAPHICS program (Centurion XVII, trial version 7.0.3, Stat Ease, USA). Accordingly, pH (range 3–7), adsorbent dosage (Fe_3O_4/Zn–Fe LDH/TGA: 3–8 mg) and removal time (range 15–45 min) were selected as effective parameters on Hg^{2+} removal, and for these three variables, α value was obtained 1.68. These parameters and their levels in the rotatable three-level CCD are shown in Table 7. According to the design, 19

Table 7 Examined levels of factors and star points of the CCD

Parameters		$-\alpha$	−1	0	1	$+\alpha$
pH	A	1.5	3	5	7	8.5
Adsorbent dosage(mg)	B	1.5	3	5.5	8	9.5
Removal time (min)	C	5	15	30	45	55

runs (including five replicates at the central point) are determined for obtaining the optimized points of each parameter, and the conditions of runs are listed in Table 1.

In brief, a certain amount of Fe_3O_4/Zn–Fe LDH/TGA nanoadsorbent was added into the 40 mL of Hg^{2+} standard solution (10 mg/L) and the pH was adjusted to a specified pH value with 0.1 mol/L HCl or NaOH and stirred for a determined time (according to Table 1). Then, the adsorbent was separated by a strong magnet and the value of the residual Hg^{2+} in the solution was determined by using AFS. The percentage removal of Hg^{2+} ($R\%$) was calculated according to the following Eq. (8):

$$R\% = \frac{C_I - C_R}{C_I} \times 100 \tag{8}$$

where C_I and C_R (mg/L) describe the initial and the residual concentrations of Hg^{2+} in the solution, respectively. $R\%$ was used as response at the experimental design program. By applying ANOVA analysis, the significant parameters consisting the values of R-square, adjusted R-square and mean absolute error are calculated.

Acknowledgements The authors gratefully acknowledge financial support from Standard Research Institute (Karaj, Iran).

References

Adlnasab L, Shabanian M, Ezoddin M, Maghsodi A (2017) Amine rich functionalized mesoporous silica for the effective removal of alizarin yellow and phenol red dyes from waste waters based on response surface methodology. Mater Sci Eng B Solid-State Mater Adv Technol 226:188–198. https://doi.org/10.1016/j.mseb.2017.09.017

Afshar E, Mohammadi-Manesh H, Dashti Khavidaki H (2017) Removal of Hg(I) and Hg(II) ions from aqueous solutions, using TiO_2 nanoparticles. Pollution 3:505–516. https://doi.org/10.7508/pj.2017.03.014

Ali J, Wang H, Ifthikar J, Khan A, Wang T, Zhan K et al (2018) Efficient, stable and selective adsorption of heavy metals by thio-functionalized layered double hydroxide in diverse types of water. Chem Eng J 332:387–397. https://doi.org/10.1016/j.cej.2017.09.080

Alimohammady M, Jahangiri M, Kiani F, Tahermansouri H (2017) Highly efficient simultaneous adsorption of Cd(II), Hg(II) and As(III) ions from aqueous solutions by modification of graphene oxide with 3-aminopyrazole: central composite design optimization. New J Chem 41:8905–8919. https://doi.org/10.1039/C7NJ01450C

Asiabi H, Yamini Y, Shamsayei M, Tahmasebi E (2017) Highly selective and efficient removal and extraction of heavy metals by layered double hydroxides intercalated with the diphenylamine-4-sulfonate: a comparative study. Chem Eng J 323:212–223. https://doi.org/10.1016/j.cej.2017.04.096

Asiabi H, Yamini Y, Shamsayei M, Molaei K, Shamsipur M (2018) Functionalized layered double hydroxide with nitrogen and sulfur co-decorated carbondots for highly selective and efficient removal of soft Hg^{2+} and Ag^{+} ions. J Hazard Mater 357:217–225. https://doi.org/10.1016/j.jhazmat.2018.05.055

Chen L, Xu H, Xie J, Liu X, Yuan Y, Liu P, Qu Z, Yan N (2019) $[SnS_4]^{4-}$ clusters modified MgAl-LDH composites for mercury ions removal from acid wastewater. Environ Pollut 247:146–154. https://doi.org/10.1016/j.envpol.2018.12.009

Cui L, Wang Y, Gao L, Hu L, Yan L, Wei Q, Du B (2015) EDTA functionalized magnetic graphene oxide for removal of Pb(II), Hg(II) and Cu(II) in water treatment: adsorption mechanism and separation property. Chem Eng J 281:1–10. https://doi.org/10.1016/j.cej.2015.06.043

Daud M, Kamal MS, Shehzad F, Al-Harthi MA (2016) Graphene/layered double hydroxides nanocomposites: a review of recent progress in synthesis and applications. Carbon 104:241–252. https://doi.org/10.1016/j.carbon.2016.03.057

Duan S, Tang R, Xue Z, Zhang X, Zhao Y, Zhang W et al (2015) Effective removal of Pb(II) using magnetic $Co_{0.6}Fe_{2.4}O_4$ microparticles as the adsorbent: synthesis and study on the kinetic and thermodynamic behaviors for its adsorption. Colloids Surf A Physicochem Eng Asp 469:211–223. https://doi.org/10.1016/j.colsurfa.2015.01.029

Esfandiyari T, Nasirizadeh N, Dehghani M, Ehrampoosh MH (2017) Graphene oxide based carbon composite as adsorbent for Hg removal: preparation, characterization, kinetics and isotherm studies. Chin J Chem Eng 25:1170–1175. https://doi.org/10.1016/j.cjche.2017.02.006

Ghasemi E, Heydari A, Sillanpää M (2017) Superparamagnetic Fe_3O_4@EDTA nanoparticles as an efficient adsorbent for simultaneous removal of Ag(I), Hg(II), Mn(II), Zn(II), Pb(II) and Cd(II) from water and soil environmental samples. Microchem J 131:51–56. https://doi.org/10.1016/j.microc.2016.11.011

Ghitescu R-E, Volf I, Carausu C, Bühlmann A-M, Gilca IA, Popa VI (2015) Optimization of ultrasound-assisted extraction of polyphenols from spruce wood bark. Ultrason Sonochem 22:535–541. https://doi.org/10.1016/j.ultsonch.2014.07.013

González MA, Pavlovic I, Rojas-Delgado R, Barriga C (2014) Removal of Cu^{2+}, Pb^{2+} and Cd^{2+} by layered double hydroxide-humate hybrid sorbate and sorbent comparative studies. Chem Eng J 254:605–611. https://doi.org/10.1016/j.cej.2014.05.132

Jainae K, Sukpirom N, Fuangswasdi S, Unob F (2015) Adsorption of Hg(II) from aqueous solutions by thiol-functionalized polymer-coated magnetic particles. J Ind Eng Chem 23:273–278. https://doi.org/10.1016/j.jiec.2014.08.028

Jamshidi M, Ghaedi M, Dashtian K, Hajati S (2015) New ion-imprinted polymer-functionalized mesoporous SBA-15 for selective separation and preconcentration of Cr(III) ions: modeling and optimization. RSC Adv 5:105789–105799. https://doi.org/10.1039/C5RA17873H

Jawad A, Peng L, Liao Z, Zhou Z, Shahzad A, Ifthikar J, Zhao M, Chen Z, Chen Z (2019) Selective removal of heavy metals by hydrotalcites as adsorbents in diverse wastewater: different intercalated anions with different mechanisms. J Clean Prod 211:1112–1126. https://doi.org/10.1016/j.jclepro.2018.11.234

Kokkinos E, Simeonidis K, Zouboulis A, Mitrakas M (2015) Mercury removal from drinking water by single iron and binary iron-manganese oxyhydroxides. Desalin Water Treat 54:2082–2090. https://doi.org/10.1080/19443994.2014.934105

Laipan M, Fu H, Zhu R, Sun L, Zhu J, He H (2017) Converting spent Cu/Fe layered double hydroxide into Cr(VI) reductant and porous carbon material. Sci Rep 7:7277. https://doi.org/10.1038/s41598-017-07775-8

Li L, Fan L, Sun M, Qiu H, Li X, Duan H et al (2013) Adsorbent for chromium removal based on graphene oxide functionalized with magnetic cyclodextrin–chitosan. Colloids Surf B Biointerfaces 107:76–83. https://doi.org/10.1016/j.colsurfb.2013.01.074

Li Y, Xia M, An F, Ma N, Jiang X, Zhu S et al (2019) Superior removal of Hg(II) ions from wastewater using hierarchically porous, functionalized carbon. J Hazard Mater 371:33–41. https://doi.org/10.1016/j.jhazmat.2019.02.099

Liu Y, Chen M, Yongmei H (2013) Study on the adsorption of Cu(II) by EDTA functionalized Fe_3O_4 magnetic nano-particles. Chem Eng J 218:46–54. https://doi.org/10.1016/j.cej.2012.12.027

Maghsodi A, Adlnasab L (2019) In-situ chemical deposition as a new method for the preparation of Fe_3O_4 nanopaeticles embedded on anodic aluminum oxide membrane (Fe_3O_4@AAO): characterization and application for arsenic removal using response surface methodology. J Environ Chem Eng 7:103288. https://doi.org/10.1016/j.jece.2019.103288

Maghsodi A, Adlnasab L, Shabanian M, Javanbakht M (2018) Optimization of effective parameters in the synthesis of nanopore anodic aluminum oxide membrane and arsenic removal by prepared magnetic iron oxide nanoparicles in anodic aluminum oxide membrane via ultrasonic-hydrothermal method. Ultrason Sonochem 48:441–452. https://doi.org/10.1016/j.ultsonch.2018.07.003

Maia LFO, Hott RC, Ladeira PCC, Batista BL, Andrade TG, Santos MS et al (2019) Simple synthesis and characterization of L-cystine functionalized δ-FeOOH for highly efficient Hg(II) removal from contamined water and mining waste. Chemosphere 215:422–431. https://doi.org/10.1016/j.chemosphere.2018.10.072

Manos MJ, Kanatzidis MG (2016) Metal sulfide ion exchangers: superior sorbents for the capture of toxic and nuclear waste-related metal ions. Chem Sci 7:4804–4824. https://doi.org/10.1039/C6SC01039C

Maran JP, Nivetha CV, Priya B, Al-Dhabi NA, Ponmurugan K, Manoj JJB (2016) Modeling of polysaccharide extraction from *Gossypium arboreum* L. seed using central composite rotatable design. Int J Biol Macromol 86:857–864. https://doi.org/10.1016/j.ijbiomac.2016.01.094

Montgomery DC (1997) Design and analysis of experiments. Wiley, New York. ISBN 978-1-119-66538-0

Moradi O (2011) The removal of ions by functionalized carbon nanotube: equilibrium, isotherms and thermodynamic studies. Chem Biochem Eng Q 25:229–240

Moustafa YM, Morsi RE, Fathy M (2014) Mercury removing capacity of multiwall carbon nanotubes as detected by cold vapor atomic absorption spectroscopy: kinetic & equilibrium studies. World Acad Sci Eng Technol Int J Chem Mol Nucl Mater Met Eng 8:724–730. https://doi.org/10.5281/zenodo.1097036

Narin I, Soylak M, Elci L, Dogan M (2001) Separation and enrichment of chromium, copper, nickel and lead in surface seawater samples on a column filled with Amberlite XAD-2000. Anal Lett 34:1935–1947. https://doi.org/10.1081/AL-100106123

Naushad M, Ahamad T, AlOthman ZA, Ala'a H (2019) Green and eco-friendly nanocomposite for the removal of toxic Hg(II) metal ion from aqueous environment: adsorption kinetics & isotherm modelling. J Mol Liq 279:1–8. https://doi.org/10.1016/j.molliq.2019.01.090

Pan S, Zhang Y, Shen H, Hu M (2012) An intensive study on the magnetic effect of mercapto-functionalized nano-magnetic Fe_3O_4 polymers and their adsorption mechanism for the removal of Hg(II) from aqueous solution. Chem Eng J 210:564–574. https://doi.org/10.1016/j.cej.2012.09.016

Peligro FR, Pavlovic I, Rojas R, Barriga C (2016) Removal of heavy metals from simulated wastewater by in situ formation of layered double hydroxides. Chem Eng J 306:1035–1040. https://doi.org/10.1016/j.cej.2016.08.054

Periyasamy S, Gopalakannan V, Viswanathan N (2017) Fabrication of magnetic particles imprinted cellulose based biocomposites for chromium(VI) removal. Carbohydr Polym 174:352–359. https://doi.org/10.1016/j.carbpol.2017.06.029

Rai A, Mohanty B, Bhargava R (2016) Supercritical extraction of sunflower oil: a central composite design for extraction variables. Food Chem 192:647–659. https://doi.org/10.1016/j.foodchem.2015.07.070

Roosta MA, Ghaedi MA, Shokri N, Daneshfar A, Sahraei R, Asghari A (2014) Optimization of the combined ultrasonic assisted/adsorption method for the removal of malachite green by gold nanoparticles loaded on activated carbon: experimental design. Spectrochim Acta A Mol Biomol Spectrosc 118:55–65. https://doi.org/10.1016/j.saa.2013.08.082

Roosta M, Ghaedi M, Asfaram A (2015) Simultaneous ultrasonic-assisted removal of malachite green and safranin O by copper nanowires loaded on activated carbon: central composite design optimization. RSC Adv 5:57021–57029. https://doi.org/10.1039/C5RA03519H

Sarma D, Islam SM, Subrahmanyam KS, Kanatzidis MG (2016) Efficient and selective heavy metal sequestration from water by using layered sulfide $K_{2x}Sn_{4-x}S_{8-x}$ (x = 065–1; KTS-3). J Mater Chem A 4:16597–16605. https://doi.org/10.1039/C6TA06404C

Shadbad MJ, Mohebbi A, Soltani A (2011) Mercury(II) removal from aqueous solutions by adsorption on multi-walled carbon nanotubes. Korean J Chem Eng 28:1029–1034. https://doi.org/10.1007/s11814-010-0463-5

Song J, Oh H, Kong H, Jang J (2011) Polyrhodanine modified anodic aluminum oxide membrane for heavy metal ions removal. J Hazard Mater 187:311–317. https://doi.org/10.1016/j.apsusc.2010.12.156

Soylak M, Narin I, Dogan M (1997) Trace enrichment and atomic absorption spectrometric determination of lead, copper, cadmium and nickel in drinking water samples by use of an activated carbon column. Anal Lett 30:2801–2810. https://doi.org/10.1080/00032719708001823

Soylak M, Elci L, Dogan M (1999) Flame atomic absorption spectrometric determination of cadmium, cobalt, copper, lead and nickel in chemical grade potassium salts after an enrichment and separation procedure. J Trace Microprobe T 17:149–156

Sumanth Kumar D, Jai Kumar B, Mahesh HM (2016) Optical properties of colloidal aqueous synthesized 3 mercaptopropionic acid stabilized CdS quantum dots. In: American Institute of physics conference series. https://doi.org/10.1063/1.4946213

Sun M, Cheng G, Ge X, Chen M, Wang C, Lou L, Xu X (2018) Aqueous Hg(II) immobilization by chitosan stabilized magnetic iron sulfide nanoparticles. Sci Total Environ 621:1074–1083. https://doi.org/10.1016/j.scitotenv.2017.10.119

Tahermansouri H, Ahi RM, Kiani F (2014) Kinetic, equilibrium and isotherm studies of cadmium removal from aqueous solutions by oxidized multi walled carbon nanotubes and the functionalized ones with thiosemicarbazide and their toxicity investigations: a comparison. J Chin Chem Soc 61:1188–1198. https://doi.org/10.1002/jccs.201400197

Tan Z, QiuJ ZengH, Liu H, Xiang J (2011) Removal of elemental mercury by bamboo charcoal impregnated with H_2O_2. Fuel 90:1471–1475. https://doi.org/10.1016/j.fuel.2010.12.004

Tang J, Huang Y, Gong Y, Lyu H, Wang Q, Ma J (2016) Preparation of a novel graphene oxide/Fe–Mn composite and its application for aqueous Hg(II) removal. J Hazard Mater 316:151–158. https://doi.org/10.1016/j.jhazmat.2016.05.028

Tekin K, Akalın MK, Şeker MG (2015) Ultrasound bath-assisted extraction of essential oils from clove using central composite design. Ind Crops Prod 77:954–960. https://doi.org/10.1016/j.indcrop.2015.09.071

Thangaraj B, Jia Z, Dai L, Liu D, Du W (2016) Lipase NS81006 immobilized on Fe_3O_4 magnetic nanoparticles for biodiesel production. Ovidius Univ Ann Chem 27:13–21. https://doi.org/10.1515/auoc-2016-0008

Wang Z, Xu J, Hu Y, Zhao H, Zhou H, Liu Y, Lou Z, Xu X (2016) Functional nanomaterials: study on aqueous Hg(II) adsorption by magnetic Fe_3O_4@SiO_2-SH nanoparticles. J Taiwan Inst Chem Eng 60:394–402. https://doi.org/10.1016/j.jtice.2015.10.041

Wang X, Lin Y, Su Y, Zhang B, Li C, Wang H et al (2017) Design and synthesis of ternary-component layered double hydroxides for high-performance supercapacitors : understanding the role of trivalent metal ions. Electrochim Acta 225:263–271. https://doi.org/10.1016/j.electacta.2016.12.160

Yan L, Yang K, Shan R, Yan T, Wei J, Yu S et al (2015) Kinetic, isotherm and thermodynamic investigations of phosphate adsorption onto core–shell Fe_3O_4@LDHs composites with easy magnetic separation assistance. J Colloid Interface Sci 448:508–516. https://doi.org/10.1016/j.jcis.2015.02.048

Zare-Dorabei R, Ferdowsi SM, Barzin A, Tadjarodi A (2016) Highly efficient simultaneous ultrasonic-assisted adsorption of Pb(II), Cd(II), Ni(II) and Cu(II) ions from aqueous solutions by graphene oxide modified with 2,2′-dipyridylamine: central composite design optimization. Ultrason Sonochem 32:265–276. https://doi.org/10.1016/j.ultsonch.2016.03.020

Zhang W, Shi X, Zhang Y, Gu W, Li B, Xian Y (2013) Synthesis of water-soluble magnetic graphene nanocomposites for recyclable removal of heavy metal ions. J Mater Chem A 1:1745–1753. https://doi.org/10.1039/C2TA00294A

Zhang F, Song Y, Song S, Zhang R, Hou W (2015) Synthesis of magnetite–graphene oxide-layered double hydroxide composites and applications for the removal of Pb(II) and 2,4-dichlorophenoxyacetic acid from aqueous solutions. ACS Appl Mater Interfaces 7:7251–7263. https://doi.org/10.1021/acsami.5b00433

Zhang Y, Lin X, Zhou Q, Luo X (2016) Fluoride adsorption from aqueous solution by magnetic core-shell Fe_3O_4@alginate-La particles fabricated via electro-coextrusion. Appl Surf Sci 389:34–45. https://doi.org/10.1016/j.apsusc.2016.07.087

Zhou Q, Lei M, Li J, Zhao K, Liu Y (2017) Sensitive determination of bisphenol A, 4-nonylphenol and 4-octylphenol by magnetic solid phase extraction with Fe@MgAl-LDH magnetic nanoparticles from environmental water samples. Sep Purif Technol 182:78–86. https://doi.org/10.1016/j.seppur.2017.01.071